Weight Loss–Induced Plasticity of Glucose Transport and Phosphorylation in the Insulin Resistance of Obesity and Type 2 Diabetes

Katherine V. Williams,[1] Alessandra Bertoldo,[2] Paul Kinahan,[3] Claudio Cobelli,[2] and David E. Kelley[1]

We tested the hypothesis that weight loss alleviates insulin resistance in skeletal muscle within the proximal steps of glucose metabolism, namely substrate delivery, glucose transport, and glucose phosphorylation. In obese subjects with and without type 2 diabetes, in vivo skeletal muscle assessments were obtained with dynamic positron emission tomography (PET) imaging performed during euglycemic clamps at moderate hyperinsulinemia (40 mU · min^{-1} · m^{-2}), using [^{15}O]H_2O and [^{18}F]fluoro-deoxyglucose ([^{18}F]FDG) to quantify tissue perfusion and glucose metabolism. Dynamic [^{18}F]FDG PET data were analyzed using both a novel muscle-specific compartmental model and a compartmental model originally developed for the brain and often used for [^{18}F]FDG muscle image quantification. Weight loss in obese subjects with (n = 9) and without (n = 9) type 2 diabetes over a 4-month intervention was substantial (14 ± 2 kg, P < 0.05). Muscle insulin resistance, assessed by insulin-stimulated [^{18}F]FDG uptake, decreased threefold in diabetic subjects and twofold in nondiabetic subjects (P < 0.001). Kinetic parameters for [^{18}F]FDG transport and phosphorylation improved substantially in both groups, whereas tissue blood flow did not change. In particular, clinically significant weight loss fully corrected insulin resistance in type 2 diabetes at the step of glucose phosphorylation and largely, but incompletely, corrected insulin resistance at the glucose transport step. *Diabetes* 52:1619–1626, 2003

Obesity induces insulin resistance in skeletal muscle, and insulin resistance is severe in obesity complicated by type 2 diabetes (1–4). Weight loss has long been the cornerstone of therapy for type 2 diabetes (5), and recent weight loss and exercise intervention trials reinforce the value of these interventions for those at risk for type 2 diabetes (6). Past studies clearly indicate that weight loss improves insulin resistance in type 2 diabetes, increases insulin-stimulated nonoxidative glucose metabolism, and enhances the effect of insulin to inhibit endogenous glucose production and suppress lipid oxidation (7–10). From this body of data, the effects of weight loss on liver, adipose tissue, and muscle can be inferred. More direct efforts to examine tissue-specific effects of weight loss have generally entailed tissue biopsy (10–12).

Several novel in vivo methods for clinical investigation of glucose metabolism, including triple-tracer dilution (13), nuclear magnetic resonance (NMR) spectroscopy (14–16), and positron emission tomography (PET) imaging with [^{18}F]fluoro-deoxyglucose ([^{18}F]FDG) (17–21), implicate a prominent role for impaired glucose transport and phosphorylation in the pathogenesis of muscle insulin resistance. Perseghin et al. (22), using phosphorous NMR of skeletal muscle during insulin-stimulated conditions to measure concentrations of glucose-6-phosphate (G6P) in normal-weight insulin-resistant first-degree relatives of type 2 diabetic patients, found that exercise training without weight loss increased G6P, and they deduced that this was attributable to improved glucose transport and/or phosphorylation. Nuutila et al. (23), using PET imaging, showed that acute exercise increased insulin-stimulated skeletal muscle glucose uptake due to increased skeletal muscle blood flow. Both phosphorous NMR and [^{18}F]FDG PET imaging of muscle have shown that fatty acids induce insulin resistance by impairing proximal steps of glucose metabolism (1,24). Both the alleviation and exacerbation of insulin resistance indicate substantial plasticity of insulin action at the proximal steps of glucose metabolism.

In the current study, we used dynamic PET imaging to address the effects of weight loss on skeletal muscle insulin resistance in obese subjects with and without type 2 diabetes. Two tracers were used in sequence during insulin-stimulated conditions. First, [^{15}O]H_2O assessed tissue perfusion. Second, [^{18}F]FDG was used to generate time-activity curves of tracer metabolism to examine proximal steps of glucose metabolism. Tissue time-activity curves for [^{18}F]FDG are markedly altered in type 2 diabetic compared with insulin-sensitive individuals (17,19), and, as will be shown in this article, weight loss markedly altered the shape of these curves. To exploit the physiological information within these curves, a recently described four-compartment/five-rate constant (5K) model was used to assess transmembrane [^{18}F]FDG transport and phosphorylation kinetics (20,21).

From the [1]Department of Medicine, University of Pittsburgh, Pittsburgh, Pennsylvania; the [2]Department of Information Engineering, University of Padova, Padova, Italy; and the [3]Department of Radiology, University of Pittsburgh, Pittsburgh, Pennsylvania.

Address correspondence and reprint requests to Katherine V. Williams, MD, Instructor of Medicine, University of Pittsburgh School of Medicine, Division of Endocrinology and Metabolism, 810N Montefiore University Hospital, 3459 Fifth Ave., Pittsburgh, PA 15213. E-mail: williamsk@msx.dept-med.pitt.edu.

Received for publication 18 December 2002 and accepted in revised form 31 March 2003.

CT, computed tomography; G6P, glucose-6-phosphate; [^{18}F]FDG, [^{18}F]fluoro-deoxyglucose; 3K, three-compartment/three-rate constant; 5K, four-compartment/five-rate constant; MBF, muscle blood flow; NMR, nuclear magnetic resonance; PET, positron emission tomography.

TABLE 1
Clinical characteristics before and after weight loss intervention

	Type 2 diabetic subjects		Obese subjects	
	Pre–weight loss	Post–weight loss	Pre–weight loss	Post–weight loss
Weight (kg)	94 ± 3	78 ± 2*	96 ± 6	83 ± 6*
BMI (kg/m^2)	35.8 ± 0.7	30.0 ± 0.5*	34 ± 3	29.6 ± 1.5*
Fat mass (kg)	40.5 ± 1.6	29.8 ± 1.3*	40.5 ± 2.8	30.5 ± 3.3*
HbA_{1c} (%)	7.2 ± 0.4†	6.5 ± 0.5	5.2 ± 0.1	5.3 ± 0.1
Glucose (mmol/l)	8.4 ± 0.8†	7.4 ± 0.9	5.2 ± 0.2	5.1 ± 0.1
Insulin (pmol/l)	96 ± 8†	61 ± 5*	71 ± 6	51 ± 6*
Basal FFA (μmol/l)	663 ± 27	508 ± 45*	553 ± 48	521 ± 50
$V_{O_{2max}}$ (ml · FFM^{-1} · min^{-1})	37.2 ± 1.2†	38.5 ± 1.7	43.1 ± 1.1	44.6 ± 2.4

Data are means ± SE. *$P < 0.05$ compared with baseline, †$P < 0.05$ compared with obese subjects with normal glucose tolerance. FFA, free fatty acid.

RESEARCH DESIGN AND METHODS

Research volunteers. Obese subjects with and without type 2 diabetes with no medical contraindication to a very-low-calorie diet were recruited after obtaining informed consent. Subjects taking insulin, taking medications known to adversely affect glucose homeostasis, or reporting weight change of >6 kg during the prior 6 months were excluded. Subjects underwent a screening medical visit including laboratory testing. Type 2 diabetic subjects discontinued oral diabetic agents and participated if their glucose levels remained <300 mg/dl. The University of Pittsburgh institutional review board approved all study procedures.

Type 2 diabetic subjects (8 women, 1 man) were 51 ± 2 years old, and subjects with normal glucose tolerance (7 women, 2 men) were 45 ± 2 years old ($P = 0.07$ compared with diabetes). At baseline (Table 1), both groups were of comparable weight and BMI.

Weight loss intervention. Subjects met weekly with a dietitian, received an 800 kcal/day liquid meal replacement (Optifast Formula) for 12 weeks, and consumed 1,200 kcal per day during weeks 13–14. Before clamp studies, subjects followed a weight maintenance diet for at least 2 weeks, maintained an intake of at least 200 g carbohydrate for at least 3 days, and avoided exercise or strenuous exertion for 2 days.

Hyperinsulinemic-euglycemic clamp. Subjects were admitted to the University of Pittsburgh General Clinical Research Center, received a standardized dinner, and fasted overnight. An antecubital venous catheter was placed for infusion of insulin, dextrose, and PET tracers, and a radial artery catheter was placed for arterial samples. During a 4-h insulin infusion (40 mU/m^2 per min), euglycemia (90 mg/dl) was maintained with 20% dextrose. Plasma insulin levels were obtained every 30 min. Subjects were moved into the PET/computed tomography (CT) scanner 2 h after starting the insulin infusion.

CT. The SMART scanner, a combined PET (ECAT ART) and helical CT tomograph (SoMatom AR.SP; Siemens) scanned a 16.2-cm-long segment of both calves (25). The CT was used for attenuation correction of the PET image (26) and placement of regions of interest within corresponding regions of skeletal muscle imaged with PET as previously described (17).

PET imaging with [^{15}O]H_2O. For blood flow assessment, a bolus injection of [^{15}O]H_2O (45 mCi) was given, and PET imaging lasted 4 min (24 × 10 s time frames). Arterial blood sampling, controlled by a peristalsis pump and quantitated with a blood radioactivity monitor, was 10 ml/min for 90 s and then reduced to 2 ml/min.

PET imaging with [^{18}F]FDG. Allowing 10 min for decay of the [^{15}O]H_2O signal, a bolus injection of [^{18}F]FDG (4 mCi) was given, and 28 PET frames (2 × 30 s, 8 × 15 s, 4 × 30 s, 3 × 1 min, 1 × 2 min, 10 × 5 min) were obtained over 60 min. Arterial blood sampling for [^{18}F]FDG consisted of 29 hand-drawn 0.5 ml samples from a radial artery catheter (10 × 6 s, 8 × 15 s, 3 × 3 min, 5 × 10 min) over 62 min.

Compartmental modeling of PET data overview. The [^{15}O]H_2O data were analyzed using a one-tissue compartment model (27). Two parameters were estimated: *1*) muscle blood flow (MBF; ml · min^{-1} · ml^{-1}) and *2*) water efflux from the tissue, expressed as λ/MBF (min^{-1}), where λ is the distribution constant of water in the tissue. The [^{18}F]FDG kinetics were assessed with both the 5*K* muscle-specific model and the three-compartment/three-rate constant (3*K*) model originally developed for dynamic PET studies of the brain and often used for skeletal muscle studies.

5*K* model for [^{18}F]FDG. The 5*K* model (Fig. 1*A*) more specifically delineates the parameters of [^{18}F]FDG transport and phosphorylation in skeletal muscle by accounting for three kinetic steps: *1*) transport from capillaries to extracellular space; *2*) transport from extracellular space to intracellular space; and *3*) intracellular phosphorylation (20,21). The five-rate constants of the model represent the following: k_1 (ml · ml^{-1} · min^{-1}), delivery to extracellular space; k_2 (min^{-1}), efflux from the extracellular space to plasma; k_3 (min^{-1}), transport into skeletal muscle; k_4 (min^{-1}), efflux from skeletal muscle to extracellular space; and k_5 (min^{-1}), phosphorylation within skeletal muscle.

From the estimates of the five-rate constants, three additional parameters were calculated: fractional uptake of [^{18}F]FDG, *K* (ml · ml^{-1} · min^{-1}),

$$K = \frac{k_1 k_3 k_5}{k_2 k_4 + k_2 k_5 + k_3'}$$

and control coefficients of transmembrane transport, $C^T = k_5/(k_4 + k_5)$, and transmembrane phosphorylation, $C^P = k_4/(k_4 + k_5)$. The biochemical principle behind C^T and C^P is that after entry, glucose can either be trapped by

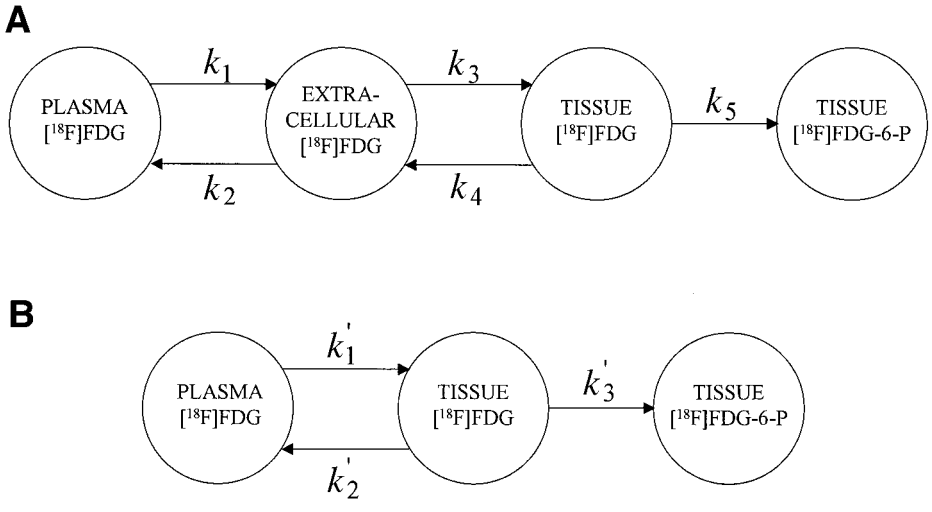

FIG. 1. The 5*K* muscle-specific model (*A*) and the 3*K* model (*B*).

TABLE 2
Insulin-stimulated systemic glucose utilization obtained from the euglycemic-hyperinsulinemic clamp

	Type 2 diabetic subjects		Obese subjects	
	Pre–weight loss	Post–weight loss	Pre–weight loss	Post–weight loss
Glucose (mmol/l)	5.2 ± 0.3	4.9 ± 0.1	4.9 ± 0.1	5.1 ± 0.1
Insulin (pmol/l)	372 ± 12	354 ± 12	432 ± 30	390 ± 24
Insulin-suppressed FFA (μmol/l)	156 ± 19*	59 ± 6†	67 ± 7	50 ± 10†
R_d (mg · FFM^{-1} · min^{-1})	3.1 ± 0.3*	6.4 ± 0.9†	7.3 ± 0.6	8.3 ± 0.6

Data are means ± SE. *$P < 0.05$ compared with obese subjects with normal glucose tolerance; †$P < 0.05$ compared with baseline. R_d, rate of glucose disposal.

phosphorylation (k_5) or exit (k_4) the cell as free glucose. If all glucose entering a myocyte is phosphorylated, transport is considered to limit the overall rate of uptake and the locus of control. In contrast, if the majority of glucose that enters the cell exits the cell without being phosphorylated, then phosphorylation can be considered the rate-limiting step or locus of control.

3*K* Model for [^{18}F]FDG. The 3*K* model (Fig. 1*B*), originally applied to [^{18}F]FDG kinetics in the brain, can be described by using three-rate constants: k_1' (ml · ml^{-1} · min^{-1}), delivery to tissue; k_2' (min^{-1}), efflux of nonmetabolized [^{18}F]FDG from tissue to plasma; and k_3' (min^{-1}), phosphorylation within tissue. From the model one can also calculate K (ml · ml^{-1} · min^{-1}),

$$K = \frac{k_1' k_3'}{k_2' + k_3'}.$$

As previously reported (20,21), the k_1' parameter primarily reflects blood flow, and the k_3' parameter reflects the combined steps of glucose transport and phosphorylation.

Parameter estimation. Compartmental modeling assumes the arterial plasma time course of tracer activity as a model input function. The parameters of the [^{15}O]H_2O and the 5*K* and the 3*K* models were estimated by weighted nonlinear least squares (28), with weights optimally chosen (20,28). The 5*K* model was successfully identified in five type 2 diabetic and four obese subjects before weight loss, and in four type 2 diabetic and nine obese subjects after weight loss. In the remaining subjects, k_4 was imprecisely resolved because of data with a high signal-to-noise ratio. In these subjects, a Bayesian approach incorporated available a priori knowledge of k_4 and identified the 5*K* model with optimal weights by maximum a posteriori probability Bayes estimation (29,30), assuming k_4 as a Gaussian variable with mean and standard deviation equal to the mean and standard deviation values of the k_4 estimates obtained in the remaining subjects.

Maximal aerobic capacity. Maximal aerobic capacity ($V_{O_{2max}}$) was assessed using a standard incremental protocol with an electronically braked cycle ergometer (ERG 601; Bosch, Stuttgart, Germany) (7).

Statistical analysis. Data are expressed as the means ± SE. ANOVA was used to compare subjects with normal glucose tolerance and those with type 2 diabetes. Weight loss changes were compared using paired *t* tests. All statistics were performed using SPSS 10.0 for Windows. A *P* value of <0.05 was considered significant.

RESULTS

Clinical effects of weight loss. Weight loss was comparable in type 2 diabetic and obese subjects (15 ± 2 and 13 ± 2 kg for diabetic and obese subjects, respectively; $P = 0.40$ for comparison between groups), representing a mean weight loss of 16 ± 2 and14 ± 2%, respectively. Pre– and post–weight loss clinical characteristics are shown in Table 1. Both groups remained overweight after weight loss (BMI 30.0 ± 0.5 and 29.6 ± 1.5 kg/m^2 in diabetic and obese subjects, respectively), and no individual achieved a BMI of <25 kg/m^2. In subjects with type 2 diabetes, levels of HbA_{1c}, fasting glucose, and fasting insulin were elevated compared with obese subjects and declined with weight loss. Basal free fatty acid levels were slightly elevated compared with obese subjects ($P = 0.06$) and declined significantly with weight loss. In obese subjects, weight loss did not change values of HbA_{1c}, fasting glucose, or free fatty acids, but fasting levels of insulin declined significantly ($P < 0.05$). Maximal aerobic capacity was lower in type 2 diabetic subjects at baseline and did not change with weight loss in either group. During the euglycemic-hyperinsulinemic clamp (Table 2), type 2 diabetic and obese subjects had comparable levels of glucose and insulin before and after weight loss. Free fatty acids were elevated in type 2 diabetic subjects, and they declined significantly in both groups after weight loss. Total-body glucose disposal was reduced in type 2 diabetic subjects before weight loss ($P < 0.001$) and improved significantly ($P < 0.01$) with weight loss. Total-body glucose disposal also improved in obese subjects, but this improvement did not reach statistical significance ($P = 0.14$).

Skeletal muscle activity curves. The dynamic PET imaging data upon which any modeling results are based are the tissue time-activity curves. Representative curves for [^{18}F]FDG in skeletal muscle are shown in Fig. 2. When comparing the patterns of [^{18}F]FDG activity at baseline, uptake occurred more slowly in type 2 diabetes and reached a lower value (Fig. 2*A*) compared with obesity (Fig. 2*B*). After weight loss, the tissue curves were markedly increased and reshaped in type 2 diabetes (Fig. 2*C*) and obesity (Fig. 2*D*). These changes were particularly evident in type 2 diabetes after weight loss because the curves had an upward convexity that was largely absent in the pre–weight loss study.

5*K* model. Effects of weight loss on skeletal muscle blood flow and [^{18}F]FDG parameters are shown in Fig. 3. Fractional skeletal muscle [^{18}F]FDG uptake, *K*, (Fig. 3*A*) was reduced at baseline in type 2 diabetic compared with obese subjects ($P < 0.01$). With weight loss, *K* tripled in type 2 diabetes ($P < 0.01$) and doubled in obesity ($P < 0.01$). Despite these marked differences in skeletal muscle [^{18}F]FDG uptake, values for skeletal muscle blood flow assessed with [^{15}O]H_2O (Fig. 3*B*) were comparable at baseline and did not change with weight loss in either group. Likewise, weight loss did not significantly affect k_1 (Fig. 3*C*) or k_2 (0.33 ± 0.06 and 0.25 ± 0.07 min^{-1} in type 2 diabetic subjects before and after weight loss; 0.34 ± 0.09 and 0.32 ± 0.07 min^{-1} in obese subjects before and after weight loss), parameters representing inward and outward delivery of [^{18}F]FDG from the vascular to the extracellular space. Values for blood flow determined by [^{15}O]H_2O highly correlated with k_1 from [^{18}F]FDG analysis ($r = 0.63$, $P < 0.01$), consistent with the concept that k_1 derived from 5*K* [^{18}F]FDG data quantification reflects blood flow (20,21).

The effects of weight loss on transport (k_3) and phosphorylation (k_5) parameters are shown in Fig. 3*D* and 3*F*. Before weight loss, k_3 was reduced in type 2 diabetic subjects compared with obese subjects, but it did not

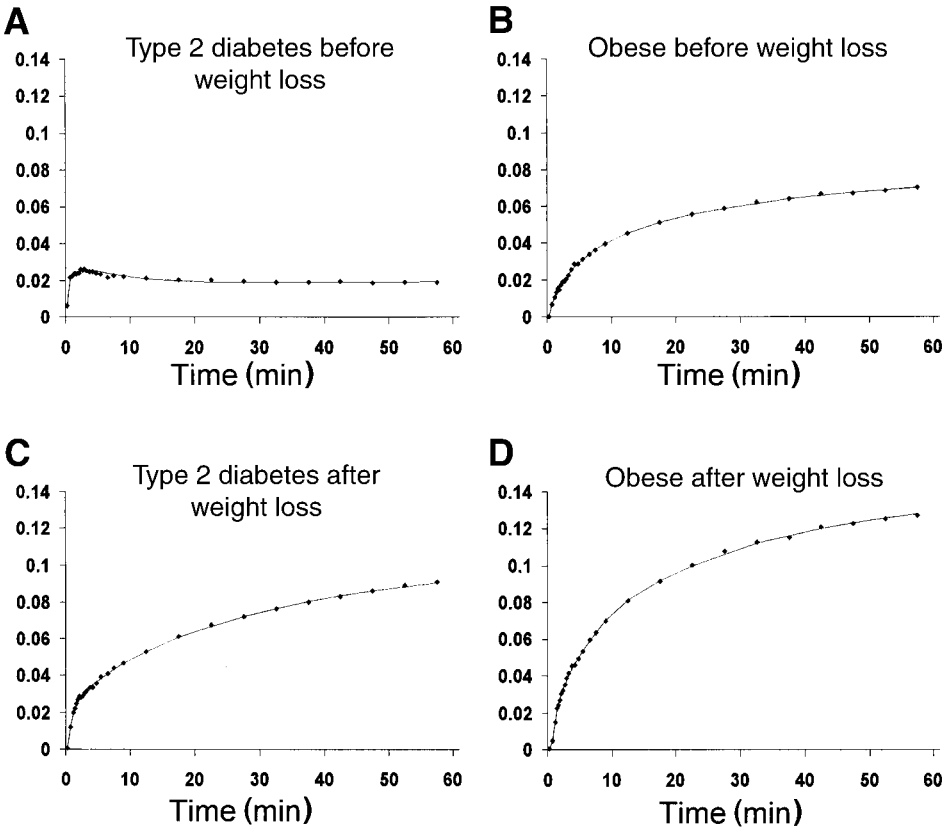

FIG. 2. Representative compartmental modeling curves for type 2 diabetes (*A* and *C*) and obese (*B* and *D*) subjects before (*A* and *B*) and after (*C* and *D*) weight loss. Dots represent observed tissue activity data for [^{18}F]FDG (μCi/ml). Lines represent the model fit.

reach statistical significance ($P = 0.10$). After weight loss, k_3 increased approximately twofold in both type 2 diabetes and obesity, with the increase in obesity reaching statistical significance ($P < 0.01$). The k_3 after weight loss in type 2 diabetes remained lower than in obesity, although this difference was not statistically significant. The rate constant for phosphorylation, k_5, was reduced in type 2 diabetic subjects at baseline compared with obese subjects ($P < 0.01$) (Fig. 3*F*). After weight loss, k_5 increased threefold in type 2 diabetes ($P < 0.001$) and by >50% in obesity ($P = 0.05$). After weight loss, k_5 was comparable in type 2 diabetes and obesity. The rate constant for outward glucose transport from skeletal muscle, k_4, was not significantly different in type 2 diabetes and obesity at baseline (Fig. 3*E*), but it decreased by more than threefold in both groups after weight loss ($P = 0.08$ for type 2 diabetic and $P < 0.05$ for obese subjects).

Before weight loss, control of glucose uptake was approximately equally distributed between transport and phosphorylation in type 2 diabetic subjects (50 ± 8% C^T, 50 ± 8% C^P) (Fig. 4*A*), whereas in obesity the control of glucose uptake resided more at the step of glucose transport (66 ± 6% C^T, 34 ± 6% C^P) (Fig. 4*B*). After weight loss, both groups had marked improvements in skeletal muscle glucose transport and phosphorylation, and the distribution of control of skeletal muscle glucose metabolism shifted strongly toward transport in both type 2 diabetes (91 ± 10% C^T, 9 ± 6% C^P) (Fig. 4*C*) and obesity (93 ± 1% C^T, 7 ± 1% C^P) (Fig. 4*D*). These findings suggest that after weight loss, phosphorylation efficiency improved so much that phosphorylation was probably no longer rate constraining, and the rate-limiting step for glucose metabolism after weight loss could largely be attributed to glucose transport.

3*K* model. Using the same [^{18}F]FDG activity curves, the 3*K* model was also applied. The fractional uptake of [^{18}F]FDG (Fig. 5*A*) exhibits the same trend demonstrated with the 5*K* analysis of the data. The parameters k_1' and k_2' (Fig. 5*B* and *C*) did not change with weight loss in type 2 diabetic or obese subjects. In addition, the k_1' values were highly correlated with skeletal blood flow values obtained from [^{15}O]H_2O analysis ($r = 0.71$, $P < 0.001$), consistent with the interpretation that these values largely reflect blood flow in skeletal muscle. Parameter k_3' (Fig. 5*D*), interpreted as an aggregate parameter reflecting both skeletal muscle glucose transport and phosphorylation, was reduced by 50% in type 2 diabetic subjects compared with those with obesity alone at pre–weight loss studies ($P < 0.05$) (Fig. 5). With weight loss, k_3' increased fivefold in type 2 diabetic subjects ($P < 0.05$) and threefold in obese subjects ($P < 0.01$).

DISCUSSION

In skeletal muscle, impaired glucose transport and phosphorylation are prominent manifestations of insulin resistance (13,15–17,19). The current investigation assessed the plasticity of these impairments in response to weight loss. Blood flow and glucose metabolism assessments with PET imaging provided a unique integrated physiological profile of the dynamics of substrate delivery, glucose transport, and phosphorylation in human skeletal muscle in response to substantial weight loss. Weight loss in obese subjects with normal glucose tolerance induced a twofold increase in insulin-stimulated [^{18}F]FDG metabolism, whereas in

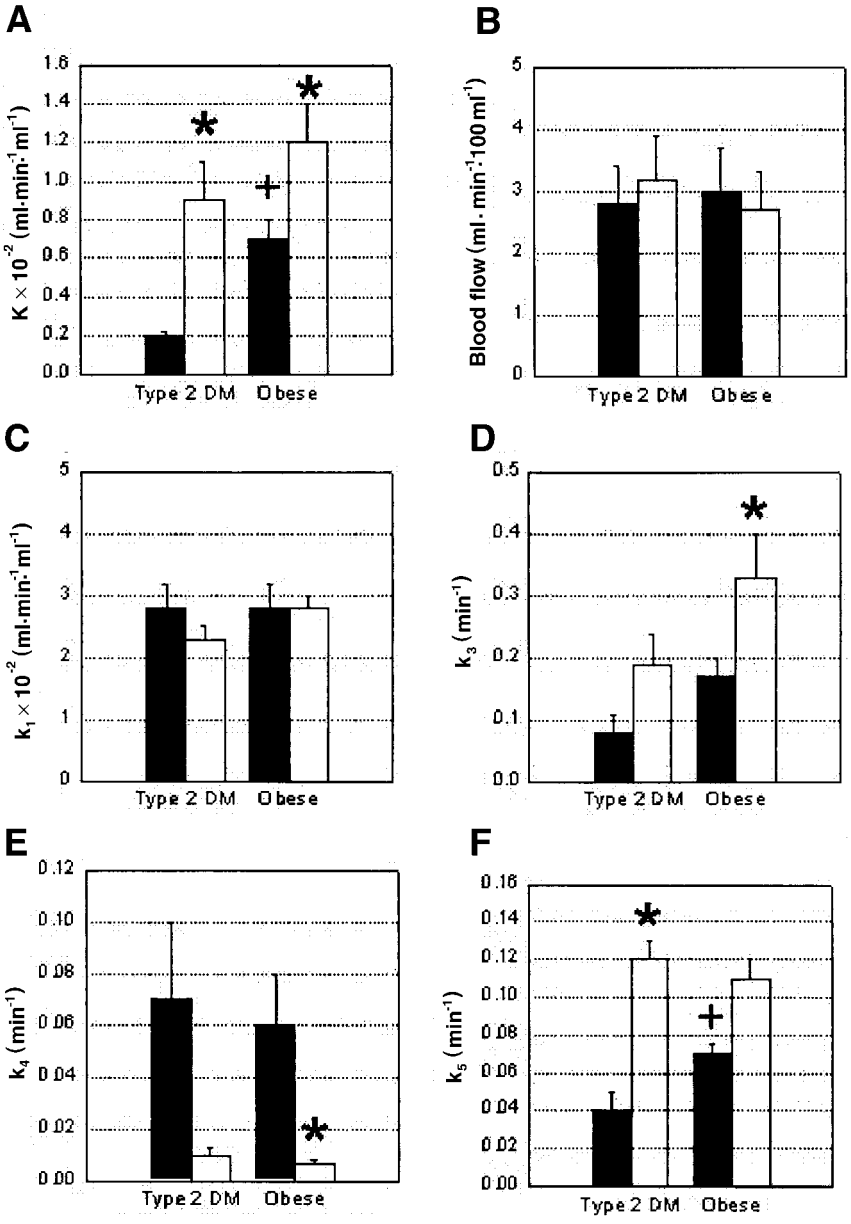

FIG. 3. Modeling results from 5*K* model. Panels show the changes in dynamic PET parameters for the following. *A*: Fractional [^{18}F]FDG uptake. *B*: Skeletal muscle blood flow. *C*: k_1, [^{18}F]FDG delivery to extracellular space. *D*: k_3, [^{18}F]FDG transport into skeletal muscle. *E*: k_4, [^{18}F]FDG transport from tissue to extracellular space. *F*: k_5, [^{18}F]FDG phosphorylation. Results are for pre–weight loss (■) and post–weight loss (□) subjects. *$P < 0.05$ compared with baseline; +$P < 0.05$ for comparison between type 2 diabetes and obese.

type 2 diabetic subjects, there was a threefold increase. Equally as dramatic were the marked changes in the configuration of the tissue time-activity curves for [^{18}F]FDG metabolism in skeletal muscle. To examine whether changes in tissue perfusion induced changes in glucose metabolism with weight loss, we used PET imaging with [^{15}O]H_2O. Consistent with our prior studies using venous occlusion plethysmography (8), weight loss increased glucose uptake in the absence of an increase in blood flow. Thus, the changes in [^{18}F]FDG tissue time-activity curves can be deduced to reflect substantial effects of weight loss on transport and phosphorylation because the metabolism of [^{18}F]FDG is substantially limited to these proximal steps of metabolism.

Two physiologically based compartmental modeling approaches of the tissue time-activity curves were used to better understand the specific effects of skeletal muscle glucose transport and phosphorylation. The 5*K* model, specifically developed for quantification of [^{18}F]FDG skeletal muscle images, indicated that weight loss had effects on both glucose transport and phosphorylation. The phosphorylation parameter was decreased in type 2 diabetic subjects before weight loss, and it was fully corrected to levels observed in obese subjects after weight loss. The glucose transport parameter also improved after weight loss, reaching statistical significance in obesity but not in type 2 diabetes. Control coefficients were estimated as an index of the distribution of control between glucose transport and phosphorylation. In healthy lean subjects during similar insulin stimulation, we find transport to be the primary loci of control, reflecting a high efficiency of glucose phosphorylation (21). In contrast, in type 2 diabetes, control was approximately equally distributed between transport and phosphorylation before weight loss. After weight loss, the rate-limiting influence of glucose transport emerges more clearly, reflecting a sharp improvement in the efficiency of glucose phosphorylation. This finding suggests that improvement in the efficiency of glucose phosphorylation is an integral aspect of the improvement of insulin resistance after weight loss in type 2

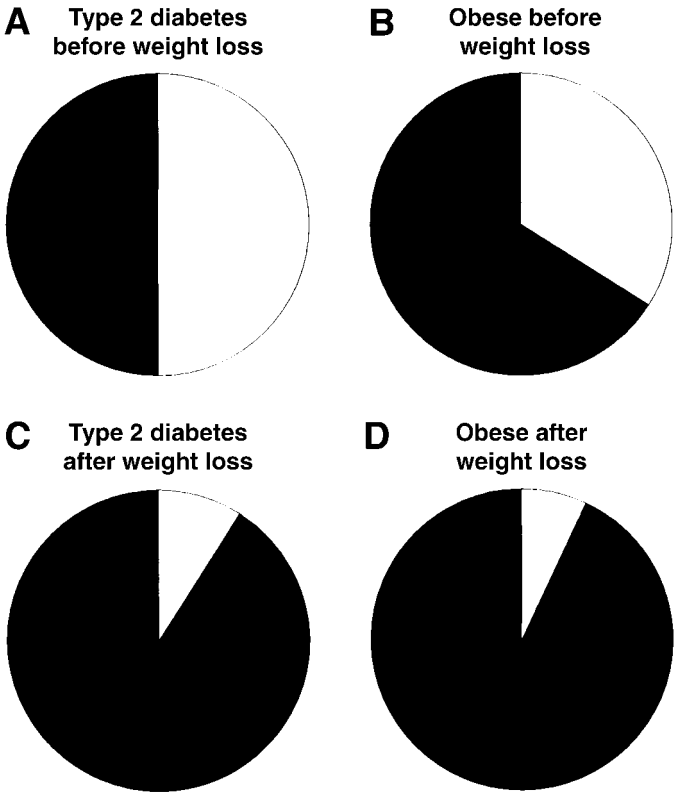

FIG. 4. Insulin-stimulated control coefficients of transmembrane transport (■) and transmembrane phosphorylation (□) in type 2 diabetic subjects (*A* and *C*) and obese subjects (*B* and *D*) before (*A* and *B*) and after (*C* and *D*) weight loss during the euglycemic-hyperinsulinemic clamp.

diabetes, and it also suggests that further alleviation of insulin resistance in type 2 diabetes could require additional improvement in the capacity for glucose transport. In those with obesity alone, in which the pre–weight loss impairment in the efficiency of glucose phosphorylation was not as great, a chief effect of weight loss was upon glucose transport, although control analyses also indicated some improvements in phosphorylation.

A three-compartment model for [^{18}F]FDG tissue kinetics, originally described for studies of deoxy-glucose metabolism by brain (31,32) and the first model used for quantification for [^{18}F]FDG kinetics in skeletal muscle (17,19,33), was also used to analyze the data. Before weight loss in obese subjects with and without type 2 diabetes, this model indicated severe impairment in the k_3' parameter, the rate constant that primarily reflects efficiency of glucose transport and phosphorylation (21). Like the k_1 values obtained using the 5*K* model, the k_1' parameter defined by this model largely reflects the transfer of [^{18}F]FDG from the plasma to a tissue compartment, and it was strongly correlated with blood flow measured independently with [^{15}O]H_2O. This further clarifies that the k_1' parameter of the 3*K* model, when applied to skeletal muscle, pertains primarily to substrate delivery, which is consistent with our prior observations (18). After weight loss, the k_1' parameter did not change; in contrast, the k_3' parameter improved threefold in obesity and five-fold in type 2 diabetes, reflecting a strong improvement in glucose transport and phosphorylation.

Several in vivo methods for the study of glucose transport and phosphorylation in skeletal muscle in humans have revealed a crucial role in the pathogenesis of insulin resistance in type 2 diabetes and obesity (13,15–17,19,20). What is unique about the current study is that we showed that inefficiencies in glucose transport and phosphorylation in type 2 diabetes and obesity can be substantially reversed with weight loss in the absence of changes in maximal aerobic capacity. In healthy subjects, induction of insulin resistance by experimental elevation of fatty acids has been shown to become manifest as impairments of glucose transport and/or phosphorylation (1,34). In a like manner, albeit in the opposite direction, the current study reveals that glucose transport and phosphorylation are central in mediating the reversal of insulin resistance. One interpretation is that impairments in glucose transport and phosphorylation may not be primary defects of insulin resistance but instead are induced impairments, or, at least, these defects have a substantial component of induced impairment.

Other studies also reveal malleability of glucose transport and phosphorylation in the reversal of insulin resistance. Recently, Greco et al. (11), found that weight loss after bariatric surgery restored GLUT4 expression in skeletal muscle and doubled insulin sensitivity in morbid obesity without type 2 diabetes. This is consistent with work from a decade ago by Friedman et al. (12), who found that after weight loss induced by gastric bypass surgery, in vitro insulin-stimulated uptake of 2-deoxyglucose in muscle fiber strips increased twofold. Henry et al. (10) also reported that weight loss doubled peripheral tissue glucose transport in type 2 diabetes by assessing ex vivo insulin-stimulated 3-*O*-methylglucose transport in adipocytes. Although it was not a weight loss study, Perseghin et al. (22) found, in an elegant study using in vivo NMR of muscle, that insulin-stimulated G6P accumulation within skeletal muscle increased twofold in the offspring of type 2 diabetic subjects in response to an exercise intervention, yet muscle glycogen synthesis remained impaired. In the current study, we cannot exclude the possibility that steps of glucose metabolism distal to blood flow, glucose transport, or its phosphorylation might contribute to some persistence of insulin resistance.

Thus, cross-sectional studies of type 2 diabetes and obesity reveal the importance of impaired glucose transport and phosphorylation in the pathophysiology of skeletal muscle insulin resistance, and they reveal that these defects can be induced quickly by elevated fatty acids. However, a more limited body of intervention-based investigations (22,23,35), of which ours is among the first to be performed with weight loss in vivo, suggest that these impairments may not be primary defects in the pathogenesis of insulin resistance. Consistent with the effects of changes in fatty acid levels to induce or alleviate insulin resistance, insulin-suppressed fatty acid levels declined in both groups in response to weight loss. The nature of the primary defect causing insulin resistance cannot be identified on the basis of the current study; however, it might be speculated based on the robust response to weight loss that was observed, and against the emerging profile of nutrient signaling that can trigger insulin resistance, that a substantial portion of the defects in glucose transport and phosphorylation arise as homeostatic adaptations to en-

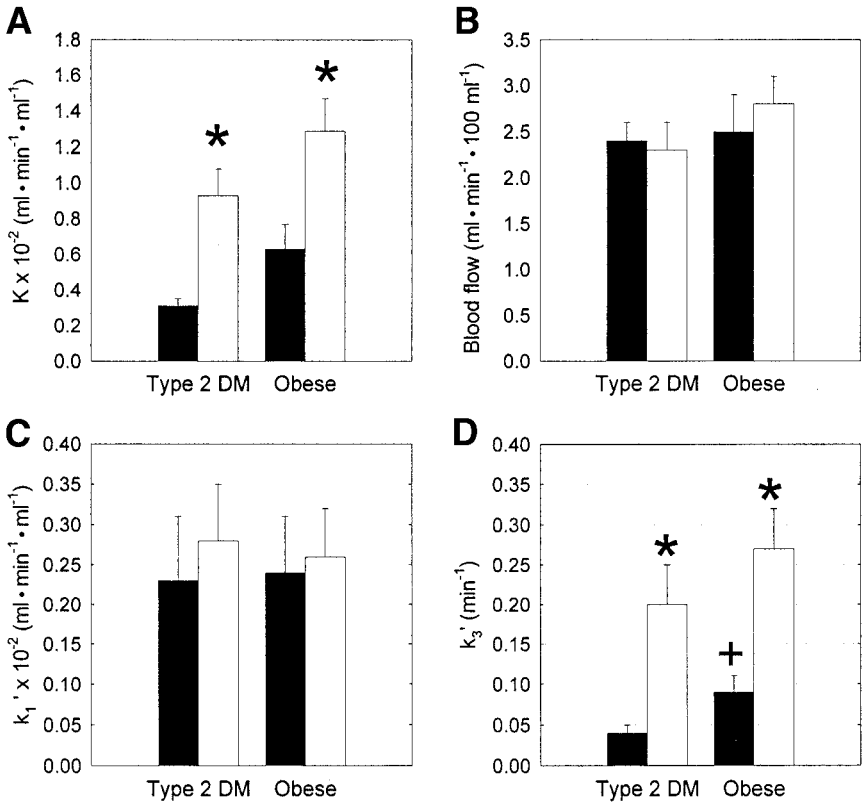

FIG. 5. Modeling results from 3*K* model. Panels show changes in dynamic PET parameters for the following. *A*: Fractional [^{18}F]FDG uptake. *B*: k_1', [^{18}F]FDG delivery. *C*: k_2', [^{18}F]FDG outward transport from tissue. *D*: k_3', [^{18}F]FDG transport/phosphorylation in tissue. Results are for pre–weight loss (■) and post–weight loss (□). **P* < 0.05 compared with baseline; +*P* < 0.05 for comparison between type 2 diabetes and obese.

ergy surplus, and they are corrected when the energy surplus is alleviated.

A limitation of the current study is the challenge of discerning roles of glucose transport and phosphorylation from single-tracer ([^{18}F]FDG) tissue time-activity curves. To address this limitation, we used [^{15}O]H_2O and were able to clarify that differences in tissue time-activity curves for [^{18}F]FDG after weight loss were not caused by changes in patterns of blood flow and tissue perfusion. Furthermore, to address the limitations of the k_1' and k_3' parameters of the 3*K* model described above, we used a recently developed muscle-specific model to more clearly distinguish between transport and phosphorylation (21). One rationale for the 5*K* addition of a separate compartment for the kinetics of the exchange of [^{18}F]FDG between the plasma compartment and the extracellular space of skeletal muscle is that skeletal muscle has a larger interstitial space than brain (36).

In summary, the current study shows that weight loss markedly improves the efficiency of skeletal muscle glucose transport and phosphorylation. The marked improvement in glucose phosphorylation in type 2 diabetes is an observation that will require further investigation to discern potential mechanisms. Weight loss had little effect on insulin-stimulated tissue perfusion or blood flow in skeletal muscle. These effects of weight loss underscore the importance of glucose transport and phosphorylation as a fulcrum of insulin resistance in skeletal muscle in type 2 diabetes and obesity, and they clearly reveal the plasticity of defects at these steps. We conclude that based on the response to weight loss, impairment in glucose transport and phosphorylation in obese subjects with and without type 2 diabetes has a substantial reactive component of impairment in the pathogenesis and treatment of insulin resistance in skeletal muscle.

ACKNOWLEDGMENTS

These studies were supported by a Mentored Patient-Oriented Research Career Development Award from the National Institutes of Health (NIH) National Institute of Diabetes and Digestive and Kidney Diseases (NIDDK; grant no. K23-DK02782), a Mid-Career Development Award for Patient Oriented Research (NIH-NIDDK Grant K24-DK02647), NIH Grant RO1-DK60555, the University of Pittsburgh General Clinical Research Center (#5MO1-RR00056), and the Obesity and Nutrition Research Center (NIH-NIDDK Grant P30-DK-46204–01). Optifast Formula was provided by Novartis Nutrition.

We gratefully acknowledge the efforts and cooperation of the research volunteers and the valuable help from the staffs of the University of Pittsburgh General Clinical Research Center and PET Center. In particular, we would like to express special appreciation to Rena R. Wing, PhD; Bret Goodpaster, PhD; David Townsend, PhD; Mary Lou Klem, PhD; Julie C. Price, PhD; Patricia H. Harper, MS, RD; Tracey Lawrence; Therese McKolanis, MPH; Christy Matan; and Jan Beattie, RN, BSN.

REFERENCES

1. Kelley DE, Williams KV, Price JC, McKolanis TM, Goodpaster BH, Thaete FL: Plasma fatty acids, adiposity, and variance of skeletal muscle insulin resistance in type 2 diabetes. *J Clin Endocrinol Metab* 86:5412–5419, 2001
2. Ludvik B, Nolan JJ, Baloga J, Sacks D, Olefsky J: Effect of obesity on insulin resistance in normal subjects and patients with NIDDM. *Diabetes* 44:1121–1125, 1995
3. Abate N, Garg A, Peshock RM, Stray-Gundersen J, Adams-Huet B, Grundy

SM: Relationship of generalized and regional adiposity to insulin sensitivity in men with NIDDM. *Diabetes* 45:1684–1693, 1996
4. Campbell P, Carlson M: Impact of obesity on insulin action in NIDDM. *Diabetes* 42:405–410, 1993
5. American Diabetes Association: Evidence-based nutrition principles and recommendations for the treatment and prevention of diabetes and related complications. *Diabetes Care* 25:S50–S60, 2002
6. Group DPPR: Reduction in the incidence of type 2 diabetes with lifestyle intervention or metformin. *N Engl J Med* 346:393–403, 2002
7. Goodpaster BH, Kelley DE, Wing RR, Meier A, Thaete FL: Effects of weight loss on regional fat distribution and insulin sensitivity in obesity. *Diabetes* 48:839–847, 1999
8. Kelley DE, Goodpaster B, Wing RR, Simoneau J-A: Skeletal muscle fatty acid metabolism in association with insulin resistance, obesity and weight loss. *Am J Physiol* 277:E1130–E1141, 1999
9. Kelley D, Wing RR, Buonocore C, Sturis J, Polonsky K, Fitzsimmons M: Relative effects of calorie restriction and weight loss in noninsulin-dependent diabetes mellitus. *J Clin Endocrinol Metab* 77:1287–1293, 1993
10. Henry RR, Wallace P, Olefsky JM: Effects of weight loss on mechanisms of hyperglycemia in obese non-insulin-dependent diabetes mellitus. *Diabetes* 35:990–998, 1986
11. Greco AV, Mingrone G, Giancaterini A, Manco M, Morroni M, Cinti S, Granzotto M, Vettor R, Camastra S, Ferrannini E: Insulin resistance with morbid obesity: reversal with intramyocellular fat depletion. *Diabetes* 51:144–151, 2002
12. Friedman JE, Dohm GL, Leggett-Frazier N, Elton CW, Tapscott EB, Pories WP, Caro JF: Restoration of insulin responsiveness in skeletal muscle of morbidly obese patients after weight loss. Effect on muscle glucose transport and glucose transporter GLUT4. *J Clin Invest* 89:701–705, 1992
13. Bonadonna RC, Del Prato S, Bonora E, Saccomani MP, Gulli G, Natali A, Frascerra S, Pecori N, Ferrannini E, Bier D, Cobelli C, DeFronzo RA: Roles of glucose transport and glucose phosphorylation in muscle insulin resistance of NIDDM. *Diabetes* 45:915–925, 1996
14. Petersen KF, Hendler R, Price T, Perseghin G, Rothman DL, Held N, Amatruda JM, Shulman GI: $^{13}C/^{31}P$ NMR studies on the mechanism of insulin resistance in obesity. *Diabetes* 47:381–386, 1998
15. Rothman DL, Magnusson I, Cline G, Gerard D, Kahn RC, Shulman RG, Shulman GI: Decreased muscle glucose transport/phosphorylation is an early defect in the pathogenesis of non-insulin-dependent diabetes mellitus. *Proc Natl Acad Sci U S A* 92:983–987, 1995
16. Rothman DL, Shulman RG, Shulman GI: P-31 nuclear magnetic resonance measurements of muscle glucose-6-phosphate: evidence for reduced insulin-dependent muscle glucose transport or phosphorylation activity in non-insulin-dependent diabetes mellitus. *J Clin Invest* 89:1069–1075, 1992
17. Williams KV, Price JC, Kelley DE: Interactions of impaired glucose transport and phosphorylation in skeletal muscle insulin resistance: a dose-response assessment using positron emission tomography. *Diabetes* 50:2069–2079, 2001
18. Kelley DE, Williams KV, Price JC: Insulin regulation of glucose transport and phosphorylation in skeletal muscle assessed by positron emission tomography. *Am J Physiol* 40:E361–E369, 1999
19. Kelley DE, Mintun MA, Watkins SC, Simoneau JA, Jadali F, Fredrickson A, Beattie J, Theriault R: The effect of non-insulin-dependent diabetes mellitus and obesity on glucose transport and phosphorylation in skeletal muscle. *J Clin Invest* 97:2705–2713, 1996
20. Bertoldo A, Peltoniemi P, Oikonen V, Knuuti J, Nuutila P, Cobelli C: Kinetic modeling of [^{18}F]FDG in skeletal muscle by PET: a four-compartment five rate constant model. *Am J Physiol* 281:E524–E536, 2001
21. Williams KV, Bertoldo A, Mattioni B, Price JC, Cobelli C, Kelley DE: Glucose transport and phosphorylation in skeletal muscle in obesity: insight from a muscle specific PET model. *J Clin Endocrinol Metab.* In Press
22. Perseghin G, Price TB, Petersen KF, Roden M, Cline GW, Gerow K, Rothman DL, Shulman GI: Increased glucose transport-phosphorylation and muscle glycogen synthesis after exercise training in insulin resistant subjects. *N Engl J Med* 335:1357–1362, 1996
23. Nuutila P, Peltoniemi P, Oikonen V, Larmola K, Kemppainen J, Takala T, Sipila H, Oksanen A, Ruotsalainen U, Bolli GB, Yki-Jarvinen H: Enhanced stimulation of glucose uptake by insulin increases exercise-stimulated glucose uptake in skeletal muscle in humans: studies using [^{15}O]O_2, [^{15}O]H_2O, [^{18}F]fluoro-deoxy-glucose, and positron emission tomography. *Diabetes* 49:1084–1091, 2000
24. Jucker BM, Rennings AJ, Cline GW, Shulman GI: ^{13}C and ^{31}P NMR studies on the effects of increased plasma free fatty acids on intramuscular glucose metabolism in the awake rat. *J Biol Chem* 272:10464–10473, 1997
25. Beyer T, Townsend DW, Brun T, Kinahan PE, Charron M, Roddy R, Israel J, Jerin J, Young J, Byars L, Nutt R: A combined PET/CT scanner for clinical oncology. *J Nucl Med* 41:1369–1379, 2000
26. Kinahan PE, Townsend DW, Beyer T, Sashin D: Attenuation correction for a combined 3D PET/CT scanner. *Med Physics* 25:2046–1053, 1998
27. Ketty SS: The theory and applications of the exchange of inert gas at the lungs and tissues. *Pharmacol Rev* 3:1–41, 1951
28. Cobelli C, Foster D, Toffolo G: *Tracer Kinetics in Biomedical Research: From Data to Model*. New York, Kluwer Academic/Plenum, 2001
29. Walter E, Pronzato L: *Identification of Parametric Models from Experimental Data*. Berlin, Springer-Verlag, 1997
30. Cobelli C, Caumo A, Omenetto M: Minimal model SG overestimation and underestimation: improved accuracy by a Bayesian two-compartment model. *Am J Physiol* 277:E481–E488, 1999
31. Phelps ME, Huang SC, Hoffman EJ, Selin CE, Sokoloff L, Kuhl DE: Tomographic measurement of local cerebral glucose metabolic rate in humans with (F-18)2-fluoro-2-deoxy-D-glucose: validation of method. *Ann Neurol* 6:371–388, 1979
32. Sokoloff L, Reivich M, Kennedy C, Des Rosiers MH, Patlak CS, Pettigrew KD, Sakurada O, Shinohara M: The [^{14}C]deoxyglucose method for the measurement of local cerebral glucose utilization: theory, procedure, and normal values in the conscious and anesthetized albino rat. *J Neurochem* 28:897–916, 1977
33. Reinhardt M, Beu M, Vosberg H, Herzog H, Hubinger A, Reinauer H, Muller-Gartner H-W: Quantitation of glucose transport and phosphorylation in human skeletal muscle using FDG PET. *J Nucl Med* 40:977–985, 1999
34. Roden M, Price TB, Perseghin G, Petersen KF, Rothman DL, Cline GW, Shulman GI: Mechanism of free fatty acid-induced insulin resistance in humans. *J Clin Invest* 97:2859–2865, 1996
35. Peltoniemi P, Yki-Jarvinen H, Oikonen V, Oksanen A, Takala TO, Ronnemaa T, Erkinjuntti M, Knuuti MJ, Nuutila P: Resistance to exercise-induced increase in glucose uptake during hyperinsulinemia in insulin-resistant skeletal muscle of patients with type 1 diabetes. *Diabetes* 50:1371–1377, 2001
36. Guyton A: *Textbook of Medical Physiology*. Philadelphia, W.B. Saunders, 1981